

Stimuli-triggered reversible switching mechanism between *H*- and *J*-type supramolecular assemblies of cationic porphyrins adsorbed on tungsten(VI) oxide surface

Kenta Adachi^{a,b*}, Yukimasa Ura^a and Naoya Kanetada^c

^aDepartment of Chemistry, Graduate School of Sciences & Technology for Innovation, Yamaguchi University, Yamaguchi, 753-8512, Japan

^bOpto-Energy Research Center, Yamaguchi University, Yamaguchi, 753-8511, Japan

^cDepartment of Environmental Science & Engineering, Graduate School of Science & Engineering, Yamaguchi University, Yamaguchi, Japan

Received 9 January 2018

Accepted 28 February 2018

ABSTRACT: Supramolecular organic dye–inorganic semiconductor nanocrystal assemblies are potentially useful in a broad range of technologies and applications, including photovoltaic systems, but the molecular basis of the adsorption of dye molecules onto the semiconductor surfaces remains poorly understood. Herein, we investigated the pH-dependent adsorption and conformational change of two cationic porphyrin stereoisomers [5,10-diphenyl-15,20-di(*N*-methyl-4-pyridyl)porphyrin (*cis*-DMPyP) and 5,15-diphenyl-10,20-di(*N*-methyl-4-pyridyl)porphyrin (*trans*-DMPyP)] on the tungsten(VI) oxide (WO₃) colloid nanoparticle in aqueous media by means of UV-vis absorption spectroscopy. In accordance with the combination of a modified Langmuir adsorption model and Kasha's exciton coupling model, the molecular orientation and stacking arrangement of DMPyP derivatives on the WO₃ colloid surface are discussed in detail. In the *trans*-DMPyP/WO₃ aqueous system, *trans*-DMPyP molecules adopted flat-on orientation with respect to the WO₃ colloid surface and eventually formed head-to-tail *J*-dimers regardless of pH conditions. *cis*-DMPyP molecules in the acidic system also lay flat-on and mainly formed *J*-dimers on the WO₃ colloid surface, whereas ones in the neutral system exhibited a dominant edge-on orientation and had a higher tendency to form face-to-face *H*-dimers. Additionally, we have also convincingly demonstrated the pH-triggered switchable π -stacking geometry of *cis*-DMPyP molecules from *H*- to *J*-dimer and vice versa on the WO₃ colloid surface. Such findings will undoubtedly provide a pertinent guideline for the rational design of stimuli-responsive organic-inorganic materials.

KEYWORDS: porphyrin, tungsten oxide, adsorption, aggregation, organic/inorganic hybrid material, stimuli-responsive.

INTRODUCTION

Nowadays, “aggregates,” composed of a large number of small molecules, have garnered considerable attention. That is because special traits which are not available in an individual molecule can be brought out only if molecules are assembled with each other [1–3]. Organic dye aggregates are ubiquitous in nature, and are of significant interest for

organic materials conceived by dynamic supramolecular approaches [4, 5]. For instance, chlorophyll molecules, which are structurally similar to porphyrin, aggregate with the assistance of robust scaffold proteins into ring-shaped and rod-like dye oligomers in purple and green bacteria, respectively [6]. In these supramolecular organizations, the porphyrin skeletons are assembled in a suitable spatial arrangement and orientation, which enables efficient energy transfer between the donor and acceptor chromophores upon photoexcitation [7]. This kind of porphyrinoid aggregate is the so-called “light-harvesting

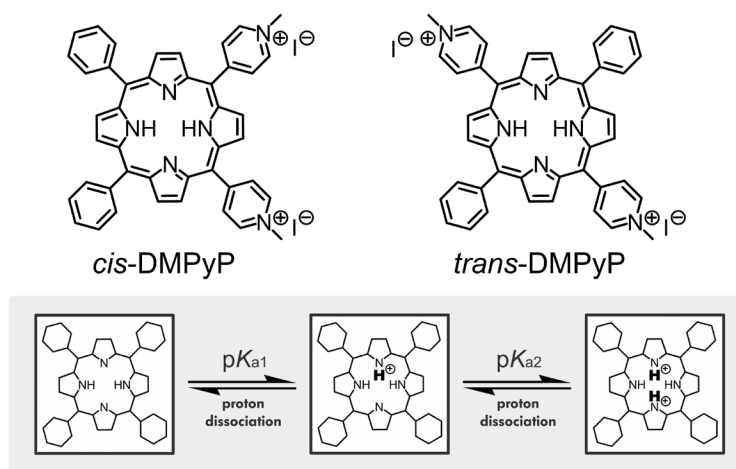
* correspondence to: Kenta Adachi, email k-adachi@yamaguchi-u.ac.jp; tel. & fax: +81 83 933 5731.

system” in photosynthetic organisms. For artificial photosynthetic systems, it is also an issue of paramount importance to design the aggregate structure of porphyrins [8]. The arrangement and orientation of organic dyes’ aggregates could be affected by many factors such as the temperature, pH, ionic strength, concentration of the dyes, and additives in the solution [9–12]. Recently, several porphyrin-based supramolecular nanostructures have been successfully assembled in a solution by using various surfactants as a structure-directing template [13, 14]. Stimuli-responsive materials are gaining attention across many different fields because of their potential applications in the environmental, biomedical, chemical, industrial, and pharmaceutical fields [15–17]. Among these materials, a large number of organic dyes’ supramolecular assemblies in response to external stimuli have been also achieved and reported [18]. However, it remains an unbeatable challenge to find more and more effective ways to achieve a fully external stimuli-controlled reversible aggregation of organic dye molecules. Generally, dye aggregates through the cooperative effect of weak intermolecular non-covalent interactions such as hydrogen bond, π - π stacking, van der Waals, and electrostatic attractive/repulsive interaction exhibit flexibility, which may be significant for a microscopic transformation of the molecular stacking [19, 20]. If one can modulate the arrangement and orientation of chromophores in the supramolecular nanostructures by external stimuli, such dye-aggregates will show changes in optical and electronic properties in response to the corresponding stimuli.

Since the integration of organic and inorganic matter is a promising way to exploit favorable properties of both material classes and to achieve novel light-emitting, sensing, photovoltaic, and lasing properties, active research is now underway to better understand organic/inorganic hybrid structures consisting of an organic dye and an inorganic semiconducting or metallic nanocrystal [21–23]. Organic dyes adsorbed on the inorganic material surface can be easily aggregated and have different orientations of their chromophores with respect to the surface (*i.e.* flat-on or edge-on) [24–26]. Of particular interest is the use of highly-ordered dye aggregates as organic components of hybrid conjugates, because dye aggregate formation on the inorganic semiconductor surfaces has been demonstrated to affect strongly the electronic and optical properties of organic chromophores in hybrid organic/inorganic photovoltaic devices such as a dye-sensitized solar cells (DSSC). In our previous studies, the adsorption/aggregation behaviors of cationic phenothiazine and xanthenes dyes on the inorganic semiconductor surface were favored by controlling the pH and ionic strength in the aqueous solution and by substituent(s) introduction and modification

in the dye molecule [27–29]. As a further step toward the tailored functional design of the organic-inorganic assemblies, it is worthwhile to investigate the adsorption/aggregation process of porphyrin derivatives on the inorganic semiconductor surface in response to external stimuli.

In the present study, we have chosen the water-soluble porphyrin derivative and the colloidal tungsten(VI) oxide (WO_3) aqueous solution systems. WO_3 is an intensively studied representative of a group of metal-oxide semiconductors with a wide band gap (<3.0 eV), and it is well-known for its unique characteristics such as photocatalytic activity, photo- and electrochromic coatings, and microelectronic applications [30, 31]. More recently, it has been demonstrated that photochromic WO_3 and related nanocolloid particles exhibit colorimetric sensing properties for α -amino acid compounds in aqueous solutions, which will have numerous applications in continuous *in vivo* monitoring [32, 33]. Herein, we will present a comparative study of two cationic porphyrin derivatives [5,10-diphenyl-15,20-di(*N*-methyl-4-pyridyl)porphyrin (*cis*-DMPyP) and 5,15-diphenyl-10,20-di(*N*-methyl-4-pyridyl)porphyrin (*trans*-DMPyP), see Scheme 1] in the WO_3 colloid aqueous solution depending upon the pH value by means of UV-vis absorption spectroscopy. The adsorption and aggregation characteristics of DMPyP derivatives on the WO_3 colloid surface were quantitatively investigated by detailed analysis based on Langmuir adsorption and exciton coupling theory. The differences in the arrangement of DMPyP derivatives adsorbed on the surface depending upon the substituents were also evaluated. The pH-responsive switchable aggregation was achieved in the *cis*-DMPyP/ WO_3 aqueous system.



Scheme 1. Structure of *meso*-diphenyl-di(*N*-methyl-4-pyridyl) porphyrin (DMPyP) derivatives used in this study, showing the protonation equilibria of the porphyrin skeleton forming monoprotonated and diprotonated forms

EXPERIMENTAL

Materials

Sodium tungstate(VI) dihydrate ($\text{Na}_2\text{WO}_4 \cdot 2\text{H}_2\text{O}$), concentrated hydrochloric acid (conc. HCl) (Analytical Reagent, Wako Pure Chemical, Osaka, Japan), and tubular membranes with 3500 dialytic modulus (Cellu-Sep T1, Membrane Filtration Products, Inc., TX, USA) were used to prepare tungsten(VI) oxide (WO_3) colloids. The water used for all sample preparation was first distilled and then passed through a Milli-Q system (Millipore, USA), resulting in the specific resistivity of 18.2 M Ω cm. All other chemicals were of reagent grade and purchased from Nacalai Tesque Inc. (Kyoto, Japan) or Wako Pure Chemical (Osaka, Japan), and were used as received without further purification.

Preparation of size-controlled WO_3 colloid solution

Colloidal WO_3 is easily prepared by the acid-catalyzed sol-gel synthesis method in aqueous media [34]. $\text{Na}_2\text{WO}_4 \cdot 2\text{H}_2\text{O}$ (100 g, 0.3 mol) was dissolved in 100 mL of water. Adding conc. HCl (7 mL, 0.7 M) dropwise into the $\text{Na}_2\text{WO}_4 \cdot 2\text{H}_2\text{O}$ aqueous solution, a cream white deposit was formed. After efficient stirring for ca. 1 h, a colorless transparent aqueous WO_3 colloid solution (pH 3.3, 0.023 M WO_3) was eventually obtained, which was then closed in a semipermeable tubular membrane and dialyzed in a 1000-mL beaker containing Milli-Q water for a period of 8 h. The Milli-Q water was periodically replaced until chloride ions could not be detected by ion chromatography. The concentration of chloride ion in the WO_3 colloid solution was determined by using a portable-type IC analyzer (PIA-1000, Shimadzu, Japan) equipped with an anion-exchange Shim-pack IC-A3 column (Shimadzu, Japan) at 30 °C. The eluent used in this study was 4-hydroxybenzoic acid (8.0×10^{-3} M)/bis(2-hydroxyethyl)iminotris-(hydroxymethyl)methane (bis-tris; 3.2×10^{-3} M), and the flow rate was 300 $\mu\text{L}/\text{min}$.

Synthesis of cationic diphenyl-di(*N*-methyl-4-pyridyl)-substituted porphyrin (DMPyP) derivatives

According to the Rothmund–Lindsey procedure [35, 36], diphenyl-di(4-pyridinyl)porphyrin derivatives [5,10-diphenyl-15,20-di(4-pyridyl)porphyrin (*cis*-DPyP) and 5,15-diphenyl-10,20-di(4-pyridyl)porphyrin (*trans*-DPyP)] were synthesized from pyrrole condensed with 4-pyridinecarboxaldehyde and benzaldehyde in refluxing propionic acid, and the crude products were purified by silica-gel column chromatography using chloroform/methanol (30:1) as eluent. 5,10-Diphenyl-15,20-di(4-pyridyl-*N*-methyl)porphyrin diiodide (*cis*-DMPyP) and 5,15-diphenyl-10,20-di(4-pyridyl-*N*-methyl)porphyrin diiodide (*trans*-DMPyP) were prepared with methyl

iodide and the corresponding di-4-pyridyl-substituted porphyrin derivatives (*cis*-DPyP and *trans*-DPyP, respectively) according to the reported method [28]. Briefly, DPyP derivative (0.32 mmol) and excess methyl iodide (0.05 mol) were successively added to dried dimethylformamide (DMF, 100 mL) at room temperature. After being refluxed for ca. 1 h, the crude product was recrystallized from a hot methanol/diethyl ether mixture to give the required derivative as a purple powder.

***cis*-DPyP:** Yield: 3.4%; $R_f = 0.40$ (4th fraction); $^1\text{H NMR}$ (CDCl_3 , 400 MHz), δ , ppm: 9.04 (m, 4H, 2,6-position pyridyl), 8.90 (d, 2H, β -pyrrol), 8.87 (s, 2H, β -pyrrol), 8.84 (s, 2H, β -pyrrol), 8.80 (s, 2H, β -pyrrol), 8.21 (m, 2H, 4-position phenyl), 8.16 (m, 4H, 3,5-position pyridyl), 7.78 (m, 8H, 2,3,5,6-position phenyl), -2.84 (s, 2H, NH).

***trans*-DPyP:** Yield: 1.7%; $R_f = 0.68$ (3rd fraction); $^1\text{H NMR}$ (CDCl_3 , 400 MHz), δ , ppm: 9.06 (m, 4H, 2,6-position pyridyl), 8.90 (d, 4H, β -pyrrol), 8.80 (d, 4H, β -pyrrol), 8.20 (m, 2H, 4-position phenyl), 8.16 (m, 4H, 3,5-position pyridyl), 7.78 (m, 8H, 2,3,5,6-position phenyl), -2.84 (s, 2H, NH).

***cis*-DMPyP:** Yield: 83.4%; $^1\text{H NMR}$ (400 MHz, DMSO-d_6 , δ): 9.47 (m, 4H, 2,6-position pyridyl), 9.13 (s, 2H, β -pyrrol), 9.02 (m, 2H, β -pyrrol), 8.99 (m, 2H, β -pyrrol), 8.91 (s, 2H, β -pyrrol), 8.90 (m, 4H, 3,5-position pyridyl), 8.25 (m, 2H, 4-position phenyl), 7.91 (m, 8H, 2,3,5,6-position phenyl), 4.72 (s, 6H, $-\text{CH}_3$), -2.84 (s, 2H, NH); MALDI-TOF-MS m/z : 901 [*cis*-DMPyP + 2I] + H^+ ; Anal. calcd. for $\text{C}_{44}\text{H}_{34}\text{N}_6\text{I}_2$: C, 58.68; H, 3.81; N, 9.33. Found : C, 58.58; H, 3.84; N, 9.27.

***trans*-DMPyP:** Yield: 77.8%; $^1\text{H NMR}$ (400 MHz, DMSO-d_6 , δ): 9.46 (m, 4H, 2,6-position pyridyl), 9.04 (m, 4H, β -pyrrol), 9.03 (m, 4H, 3,5-position pyridyl), 8.98 (d, 4H, β -pyrrol), 8.24 (m, 2H, 4-position phenyl), 7.91 (m, 8H, 2,3,5,6-position phenyl), 4.71 (s, 6H, $-\text{CH}_3$), -2.84 (s, 2H, NH); MALDI-TOF-MS m/z : 901 [*trans*-DMPyP + 2I] + H^+ ; Anal. calcd. for $\text{C}_{44}\text{H}_{34}\text{N}_6\text{I}_2$: C, 58.68; H, 3.81; N, 9.33. Found: C, 58.45; H, 3.89; N, 9.21.

Adsorption-aggregation behaviors of DMPyP derivatives on the WO_3 colloid surface

A typical experiment would consist of first mixing the DMPyP derivative aqueous solution, water, sodium sulfate (ionic strength adjustment), and hydrochloric acid or sodium hydrate. Then the WO_3 colloid aqueous solution would be added and stirred for 10 min at room temperature. It was preliminarily established that this time is sufficient for the establishment of adsorption-aggregation equilibrium. The pH values of the DMPyP/ WO_3 aqueous solution were periodically checked with an F-14 pH meter (Horiba, Japan) equipped with a 6366-10D glass electrode (Horiba, Japan). The DMPyP/ WO_3 aqueous solution was injected into a single compartment cell (0.1 or 1.0 cm path length) with two quartz windows.

Afterward, static UV-vis absorption spectra of the DMPyP/WO₃ aqueous solution were obtained on a V-730 spectrometer (Jasco, Japan).

Other equipment

Elemental analyses were determined using a Perkin-Elmer 2400 series II CHNS/O elemental analyzer. Nitrogen adsorption-desorption isotherm was measured at -195.8 °C with a TriStar II 3020 analyzer (Micromeritics, USA). Dried WO₃ colloid samples (*ca.* 0.5 g) were prepared by evaporating water from the WO₃ colloid aqueous solution, and then outgassed with helium for 2 h at 200 °C prior to the adsorption measurement. The Brunauer-Emmett-Teller (BET) method [37] was applied to calculate the specific surface area. By using the Barrett-Joyner-Halenda (BJH) model [38], the pore-size distributions were calculated from the adsorption branch isotherms. As previously reported [29], the specific surface area is 11.8 m²·g⁻¹ and the pore size is about 50 nm. Hydrogen nuclear magnetic resonance (¹H NMR) spectra of the porphyrin derivatives were recorded on an AVANCE DPX-400 (400 MHz) spectrophotometer (Bruker, USA) with tetramethylsilane (TMS) as the internal standard. MALDI-TOF mass spectra were acquired on a Voyager DE PRO (Applied Biosystems, USA) using α-cyano-4-hydroxycinnamic acid as a matrix. The TEM image of WO₃ colloids was measured with a JEM-2000EX II instrument (JEOL, Japan). The TEM samples were prepared by dropping the WO₃ colloid sample solution onto a copper grid covered with a carbon film. The size distribution histogram of WO₃ colloids was assessed by averaging the sizes of 100 particles directly from the TEM images. The resulting samples were composed of almost spherical particles with diameters over the range 6–22 nm (see Fig. S1).

RESULTS AND DISCUSSION

Molecular forms of DMPyP derivatives in aqueous media

To theorize the nature of the interaction between DMPyP derivatives and WO₃ colloids, a detailed understanding of the behavior and habits of both *cis*- and *trans*-DMPyP in aqueous solutions is required. Two DMPyP derivatives (*cis*- and *trans*-DMPyP) were well-synthesized *via* the Rothmund–Lindsey procedure. Both DMPyP derivatives are quite soluble (>1.0 × 10⁻⁴ M) in water. At first, we studied the concentration dependence on the absorption spectra for *cis*- and *trans*-DMPyP in acidic (pH = 1.5) and neutral (pH = 6.0) aqueous solution, as shown in Fig. S2. At low concentrations of DMPyP derivatives (<1.0 × 10⁻⁶ M), the UV-vis absorption spectra in aqueous solution are dominated typically by two intense bands: the Soret band around 400–450 nm and the

weak Q bands in the visible region at about 500–700 nm, arising from the a_{1u}(π)–e_g(π) and a_{2u}(π)–e_g(π) transition [39], respectively. Under acidic conditions (pH = 1.5), the Lambert–Beer law was obeyed for both DMPyP derivatives in the concentration range from 5.0 × 10⁻⁶ to 1.0 × 10⁻⁴ M at the maximum absorption wavelength (not shown). However, the absorption spectra of DMPyP derivatives showed a nonlinear concentration dependence at neutral pH condition (pH = 6.0), *e.g.* the intensity of Soret band gradually decreased with the increase of the DMPyP concentration, and the absorption spectra showed a discernible shoulder 390 nm in higher concentration than 1.0 × 10⁻⁶ M. Some isosbestic points were observed in the visible region of their spectra, indicating that the initial and final species were in equilibrium [40]. It is well-known that porphyrin compounds tend to interact with each other by attractive π–π stacking owing to their extended flat aromatic surface [41]. Actually, the blue-shift, broadening and lowering in the intensity of Soret band clearly indicate the dimerization with a “face-to-face” arrangement. To determine the dimerization constant (K_D) of DMPyP derivatives in neutral water, the molar absorbance coefficient at maximum peak was plotted as a function of the total DMPyP concentration, assuming the following monomer and dimer equilibrium (Equations 1 and 2):



$$K_D = \frac{[(\text{DMPyP})_2]}{[\text{DMPyP}]^2} \quad (2)$$

Using the monomer molar absorbance coefficient (ε_m) obtained from the absorbance in the dilute solution (<1.0 × 10⁻⁶ M), the values of K_D and dimer molar absorbance coefficient (ε_d) for DMPyP derivatives were calculated from the curve-fitting in the inset of Fig. S2. These obtained values are listed in Table S1 (K_D: 1.25 × 10⁴ M⁻¹ for *cis*-DMPyP and 0.89 × 10⁴ M⁻¹ for *trans*-DMPyP). Interestingly, in spite of the structural similarity of the two molecules, *cis*-DMPyP molecules form more stable aggregates than *trans*-DMPyP ones.

Free-base (non-metallated) water-soluble porphyrin compounds can bind to one or two protons on pyrrolic nitrogens, resulting in the mono- and di-protonated species [42]. Generally, the porphyrin species exhibit significant spectral changes during protonation. As shown in Fig. S3, UV-vis absorption spectra of dilute *cis*- and *trans*-DMPyP aqueous solutions (1.0 × 10⁻⁶ M: the formation of DMPyP dimers in the solution can be neglected) greatly changed with the pH in a range between 1 and 6. From these spectral changes, the two acid dissociation constants (pK_{a1} and pK_{a2}) of *cis*- and *trans*-DMPyP were pK_{a1} = 3.03 and 3.08, pK_{a2} = 2.88 and 2.90, respectively, in agreement with values reported in the literature (pK_{a1} = *ca.* 3.0 and pK_{a2} = *ca.* 2.9) [43, 44]. Herein, it is noted that free-base DMPyP in neutral

water (pH 6.0) tends to form dimers even though no significant association of di-protonated DMPyP is seen in acidic aqueous media (pH 1.5). Spectral studies have demonstrated that the self-association behavior of DMPyP derivatives in water is obviously governed by the arrangement of two peripheral cationic groups on the *meso*-positions of the porphyrin ring and/or the protonation of the porphyrin core.

Adsorption and aggregation behaviors of DMPyP derivatives on the WO₃ colloid surface

The WO₃ colloid particles had a unique adsorption property for various organic dyes in an aqueous solution. Furthermore, a self-aggregation phenomenon of organic dyes adsorbed on the WO₃ colloid surface occurred, as had been reported in our previous study [10–12]. The UV-vis absorption spectra in the DMPyP/WO₃ aqueous system were measured under acidic (pH = 1.5) and neutral (pH = 6.0) conditions. Both acidic and neutral DMPyP/WO₃ aqueous solutions were essentially transparent in the visible region under the present experimental conditions, and stable for several weeks without precipitate at room temperature. As shown in Fig. 1, the addition of the WO₃ colloid aqueous solution resulted in significant spectral changes of both DMPyP derivatives in the visible region. In particular, a gradual decrease in the monomer Soret band intensity of *trans*-DMPyP was observed with a titration of the WO₃ colloid aqueous solution, along with a red-shift in absorption edge to a longer wavelength and an appearance of a new weak band at around 370 nm regardless of pH conditions (Figs 1(c) and (1d)). On

the other hand, the absorption spectral changes in the *cis*-DMPyP/WO₃ aqueous system at acidic and neutral pH were strikingly different. As the concentration of the WO₃ colloid increases, the monomer Soret band for *cis*-DMPyP decreased sharply and shifted to the longer wavelength at pH 1.5 (Fig. 1(a)), but shifted to the shorter wavelength at pH 6.0 (Fig. 1(b)). Oddly enough, both acidic and neutral *cis*-DMPyP/WO₃ aqueous systems exhibit weak red-shifted Q bands.

When small-molecule chromophores assemble in the aqueous solution, they often form *H*-type or *J*-type aggregates, depending on the relative alignment of the transition dipole moments on adjacent molecules [4, 5]. Specifically taking into account the angle between the direction of the transition dipole moments and the line linking the molecular centers (θ) and the angle between the transition dipole moments of the monomers in the aggregate (α), several specific cases can be considered (Scheme 2). In the context of Kasha's molecular exciton coupling theory [45], face-to-face stacked chromophores ($54.7^\circ < \theta \leq 90^\circ$ and $\alpha = 0$; *H*-type aggregate) are expected to exhibit a blue-shifted band (*H*-band) because only the higher energy exciton transition is allowed. On the other hand, head-to-tail arranged chromophores ($0^\circ \leq \theta < 54.7^\circ$ and $\alpha = 0$; *J*-type aggregate) exhibit a red-shifted band (*J*-band) because only the lower energy excitation is allowed. However, for a twisted face-to-face ($54.7^\circ < \theta \leq 90^\circ$ and $0^\circ < \alpha \leq 90^\circ$) or an oblique head-to-tail aggregate ($0^\circ \leq \theta < 54.7^\circ$ and $0^\circ < \alpha \leq 90^\circ$), both *H*- and *J*-bands will be observed in the absorption spectra, because both the higher and lower energy exciton transitions are allowed. In these cases, the *H*-band will

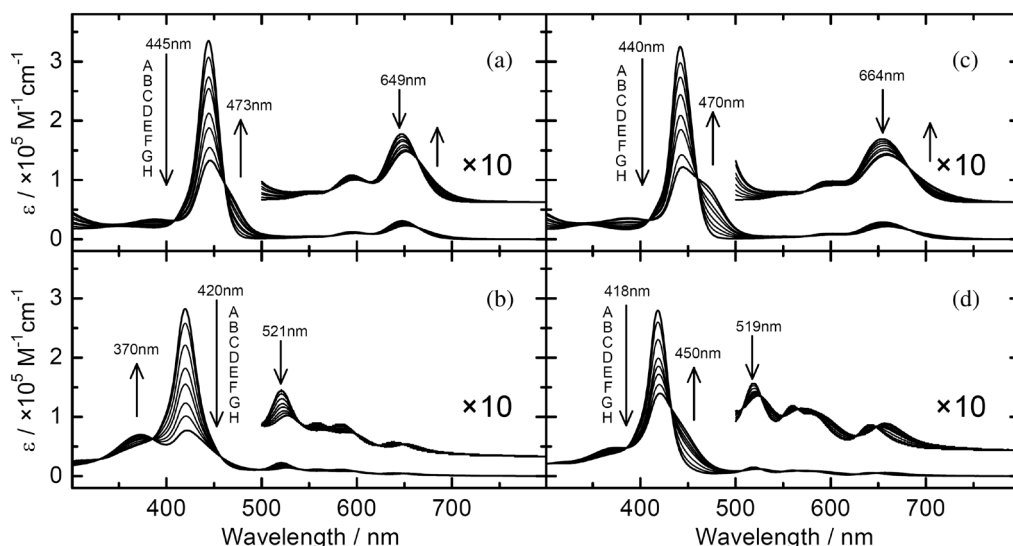
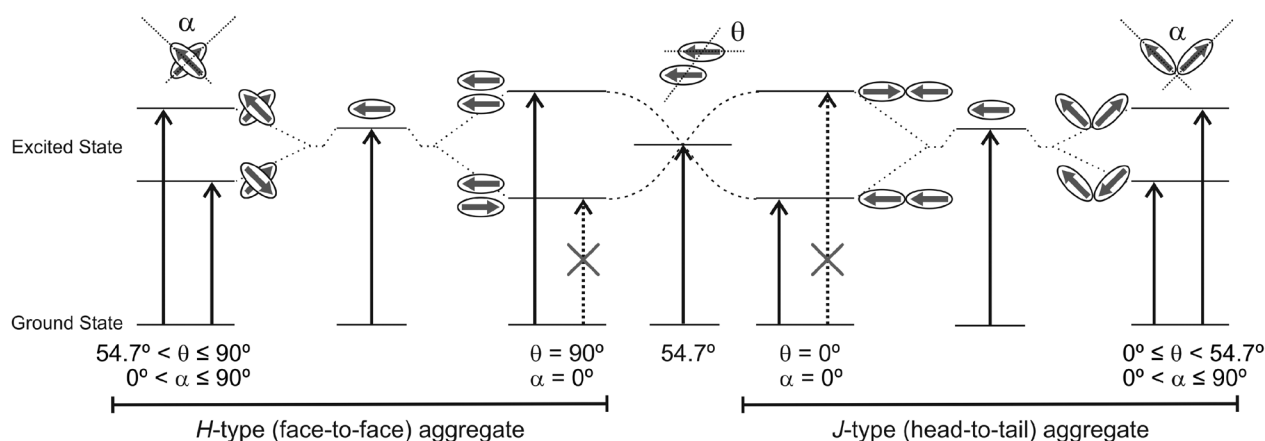


Fig. 1. Change of UV-vis absorption spectra of (a) *cis*-DMPyP in acidic water, (b) *cis*-DMPyP in neutral water, (c) *trans*-DMPyP in acidic water, and (d) *trans*-DMPyP in neutral water as a function of added WO₃ colloid at 25 °C. Concentration conditions: [DMPyP derivative] = 1.0×10^{-6} M; [Na₂SO₄] = 3.3×10^{-2} M; pH 1.5 (acidic condition), pH 6.0 (neutral condition); molar ratios ([WO₃]/[DMPyP derivative]) as follows: (A) 0, (B) 4, (C) 8, (D) 10, (E) 25, (F) 40, (G) 50, and (H) 80. The arrows indicate the direction of the absorbance changes, as the WO₃ colloid concentration is increased

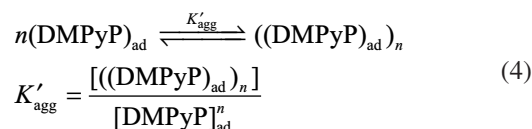
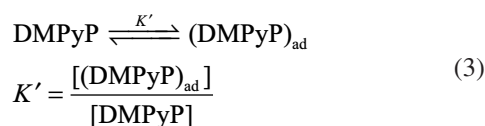


Scheme 2. Orientation dependence in exciton coupling between two chromophores (ellipses) and their electric dipoles (arrow in ellipse). The solid and dashed arrows from ground states to excited states represent allowed and forbidden transitions, respectively

be more intense for the twisted face-to-face aggregate, whereas the oblique head-to-tail aggregate is achieved if the *J*-band is more intense. In the *trans*-DMPyP/ WO_3 aqueous system, oblique *J*-aggregates were present regardless of pH conditions. Moreover, the contrasting spectral shifts in the *cis*-DMPyP/ WO_3 aqueous system indicate that *cis*-DMPyP chromophores in the acidic WO_3 colloid aqueous solution adopt the *J*-aggregation mode, whereas ones in the neutral WO_3 colloid aqueous solution exhibit *H*-aggregation tendency. It is interesting to note that the neutral *cis*-DMPyP/ WO_3 aqueous system exhibits weak red-shifted Q bands, not blue-shifted ones (see Fig. 1(b)), though the reason is not clear at the present stage. In tetrapyrrolic chromophores, the derivation and interpretation of the spectra of their aggregates are still complicated by the presence of two perpendicular dipole moments [4, 5].

Generally, metal oxide particles in an aqueous system are hydrated and M–OH groups cover their surface. The M–OH sites on the surface of particles can react with H^+ or OH^- from dissolved acids or bases, and positive (M– OH_2^+) or negative (M– O^-) charges develop on the surface. Thus, metal oxides have a characteristic pH, where the positive and negative sites are in equal amount (isoelectric point, IEP) [46]. At pH values lower than the IEP the particle surface charge is positive, and at pH values higher than the IEP, the particle surface charge is negative. Since the IEP of WO_3 is 0.2–0.5 [47], the WO_3 colloid surface is negatively charged in this aqueous solution (pH = 1.5 and 6.0). As can be seen from the above section, the aggregation (including dimerization) of DMPyP derivatives in acidic and neutral water is almost negligible under this dye concentration (1.0×10^{-6} M). On the basis of the well-known peculiarities of the physicochemical properties of metal oxide nanoparticles and cationic porphyrin derivatives in the aqueous system, we suggest that two different driving forces (the electrostatic interaction between the negatively charged WO_3 colloid surface and the peripheral cationic

anchoring groups and/or the di-protonated porphyrin core of DMPyP derivatives, and the π – π stacking interaction between the DMPyP derivatives adsorbed on the surface) can be considered as the most probable adsorption and aggregation mechanism, respectively. The adsorption and aggregation processes of DMPyP derivatives in the DMPyP/ WO_3 aqueous system need to be identified separately to quantitatively evaluate each other. Actually, stable isosbestic points were observed in the UV-vis absorption spectra during the titration experiment in which the DMPyP derivative concentration was held constant and combined with aqueous solutions of the different concentration of WO_3 colloid, implying that a sequence of adsorption and aggregation of DMPyP derivatives in the WO_3 colloid aqueous solution was proceeding apace without forming an intermediate or multiple products. Considering the dynamic equilibrium between the monomer and aggregate of the DMPyP derivative on the WO_3 colloid surface, the adsorption constant onto the WO_3 colloid surface (K') and the aggregation constant on the WO_3 colloid surface (K'_{agg}) can be defined as follows (Equations 3 and 4):



where $[\text{DMPyP}]$ and $[(\text{DMPyP})_{\text{ad}}]$ are the concentration of the DMPyP derivatives in the aqueous solution and on the WO_3 colloid surface, respectively. $[((\text{DMPyP})_{\text{ad}})_n]$ represents the concentration of the aggregate of the DMPyP derivatives on the WO_3 colloid surface. The subscript or superscript “*n*” is the apparent number of monomers in

the unit aggregate addressed in an absorption spectral change. Assuming that the concentration of monomer DMPyP derivatives on the WO_3 colloid surface is negligibly smaller than that of aggregate on the surface, the equilibrium concentration of the aggregate on the WO_3 colloid surface is spectrometrically evaluated as the following (Equation 5):

$$[(\text{DMPyP})_{\text{ad}}]_n = \frac{([\text{DMPyP}]_{\text{ini}} - [\text{DMPyP}]) \cdot V}{n \cdot S} \quad (5)$$

where the subscript 'ini' denotes initial concentration. S and V are the total surface area of the WO_3 particles (calculated using BET specific area value) and the volume of the aqueous phase, respectively. $[(\text{DMPyP})_{\text{ad}}]_n$ can be calculated from the UV-vis absorption spectra at different concentrations using the approximation method of West and Pearce [48]. Figure 2 shows apparent adsorption isotherms for DMPyP derivatives in the WO_3 colloid aqueous solution system at pH 1.5 and 6.0. These isotherm shapes were very akin to ones for the Langmuir case. In the Langmuir adsorption theory, the interaction between the species adsorbed on the surface, however, is not considered at all. Since the basic Langmuir isotherm model is not applicable in the DMPyP/ WO_3 aqueous systems, it is modified with the introduction of the aggregation constant term as the following (Equation 6):

$$[(\text{DMPyP})_{\text{ad}}]_n = \frac{K'_{\text{agg}} (aK'[\text{DMPyP}])^n}{(a + K'[\text{DMPyP}])^n} \quad (6)$$

Herein, a refers to the saturated concentration on the WO_3 colloid surface. As shown in Fig. 2, the

stoichiometric analysis of the experimental data using Equation 6 suggested the aggregation of the dimer ($n = 2$) of both *cis*- and *trans*-DMPyP on the WO_3 colloid surface, meaning that the aggregate formed on the WO_3 colloid surface must include two DMPyP molecules as a minimum number. These DMPyPs' aggregation behaviors agree with the results previously reported on the adsorption/aggregation of tetrakis(4-pyridyl)porphyrin (TPyP) derivatives on the WO_3 colloid surface [28]. In Table 1, we summarize the adsorption and aggregation (dimerization) parameters of DMPyP derivatives at two significant pH experimental conditions. Our data clearly showed that the pH in the DMPyP/ WO_3 aqueous system affected both adsorption and dimerization behaviors on the WO_3 colloid surface. In the *cis*-DMPyP/ WO_3 aqueous system, the K' value determined in acidic media is larger than the one in neutral media, whereas the K'_{agg} in acidic media is smaller than the one in neutral media. A similar tendency is also seen in the *trans*-DMPyP/ WO_3 aqueous system. As results, we find that the porphyrin core protonation is facilitated upon the adsorption of DMPyP derivatives, but prevents their dimerization reaction on the WO_3 colloid surface, which seems to be reasonable given that it would be more favorable for the stable adsorption-aggregation equilibrium in the DMPyP/ WO_3 aqueous system due to the balance of the electrostatic (attractive/repulsive) interaction between cationic DMPyP molecules and negatively charged WO_3 surface. Note that specific large saturated concentration was observed for *cis*-DMPyP at pH = 6.0. Since the absorption spectra of *cis*-DMPyP only showed hypsochromic shift on the addition of WO_3 colloid aqueous solution at neutral pH, unlike *trans*-DMPyP, the arrangement of *cis*-DMPyP molecules adsorbed on the WO_3 surface must

Table 1. Spectroscopic parameters of aggregate, saturated concentrations (a), aggregation constants ($K'_{\text{agg(dimer)}}$) of DMPyP derivatives on the WO_3 colloid surface, adsorption constants (K') onto the WO_3 colloid surface at 25 °C in two ion strength conditions, and the tilting angles (ϕ) of the porphyrin plane from the tangent line to the WO_3 particle surface.

DMPyP derivative	pH	Ion strength/ mol · dm ⁻³	$a/\text{mol dm}^{-2}$	$K'_{\text{agg(dimer)}}/\text{mol}^{-1} \cdot \text{dm}^2$	K'/dm	ϕ/degree
<i>cis</i> -DMPyP	1.5	0.01	$(0.97 \pm 0.10) \times 10^{-8}$	$(1.27 \pm 0.14) \times 10^8$	$(3.80 \pm 1.13) \times 10^{-1}$	20.3
		0.1	$(0.97 \pm 0.10) \times 10^{-8}$	$(1.27 \pm 0.14) \times 10^8$	$(2.41 \pm 0.71) \times 10^{-1}$	"
	6.0	0.01	$(2.07 \pm 0.21) \times 10^{-8}$	$(1.97 \pm 0.20) \times 10^8$	$(2.59 \pm 0.94) \times 10^{-1}$	87.2
		0.1	$(2.07 \pm 0.21) \times 10^{-8}$	$(1.97 \pm 0.20) \times 10^8$	$(1.67 \pm 0.34) \times 10^{-1}$	"
<i>trans</i> -DMPyP	1.5	0.01	$(0.98 \pm 0.12) \times 10^{-8}$	$(1.18 \pm 0.15) \times 10^8$	$(3.11 \pm 1.02) \times 10^{-1}$	20.9
		0.1	$(0.98 \pm 0.12) \times 10^{-8}$	$(1.18 \pm 0.15) \times 10^8$	$(1.91 \pm 0.58) \times 10^{-1}$	"
	6.0	0.01	$(0.96 \pm 0.17) \times 10^{-8}$	$(1.40 \pm 0.17) \times 10^8$	$(2.03 \pm 0.79) \times 10^{-1}$	22.6
		0.1	$(0.96 \pm 0.17) \times 10^{-8}$	$(1.40 \pm 0.17) \times 10^8$	$(1.25 \pm 0.39) \times 10^{-1}$	"

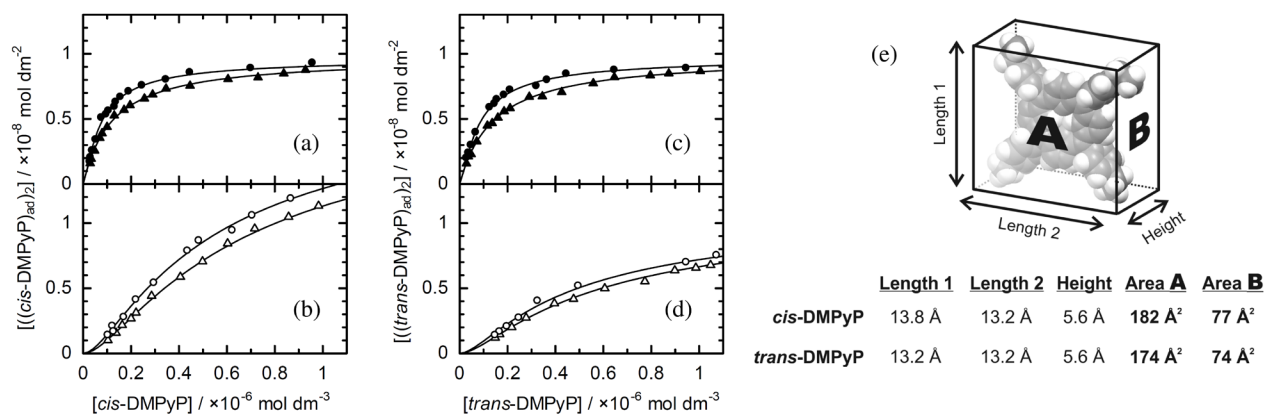


Fig. 2. Adsorption isotherms of (a) *cis*-DMPyP in acidic water, (b) *cis*-DMPyP in neutral water, (c) *trans*-DMPyP in acidic water, and (d) *trans*-DMPyP in neutral water onto the WO₃ colloid surface. Concentration conditions: [DMPyP derivative] = 1.0 × 10⁻⁶ M; [WO₃] = 1.0 × 10⁻⁶–1.0 × 10⁻³ M; [Na₂SO₄] = 3.3 × 10⁻³ M (circle), 3.3 × 10⁻² M (triangle); pH 1.5 (acidic condition), pH 6.0 (neutral condition). The solid lines are fitted by Equation 6. (e) Box approximating DMPyP derivative molecule. Areas for each face A (flat-on) and B (edge-on) were determined from the CPK model structure

be correlated to their preferred aggregate geometries on a nanoscale. The detailed information of geometrical structure in the DMPyP derivatives' aggregates formed on the WO₃ colloid surface will be argued in a later section.

Moreover, in an effort to further delineate the adsorption characteristics of the DMPyP derivatives onto the WO₃ colloid surface, we set out to quantify the influence of ionic strength on the isotherm under a constant concentration of DMPyP derivative. As shown in Fig. 2 and Table 1, the determined adsorption constants of DMPyP derivatives decreased with increasing sodium sulfate concentration. It is evident that electrostatic interactions between cationic DMPyP derivative molecules and the negatively charged WO₃ colloid surface dominate the adsorption behavior of the DMPyP derivatives on the WO₃ colloid surface.

pH-Induced switch between *H*- and *J*-aggregation mode of *cis*-DMPyP stacks on the WO₃ colloid surface

Spectroscopic discrimination between the *H*- and *J*-type dimerization modes of *cis*-DMPyP molecules in the WO₃ colloid aqueous solution was observed by UV-vis absorption spectral measurements. For novel approaches in controlling morphology and functioning of smart and promising stimuli-responsive supramolecular materials, it is worthwhile to realize that the porphyrin aggregates formed on the metal oxide would be transformed depending upon pH. Accordingly, we investigated the pH-responsive color characteristics in the *cis*-DMPyP/WO₃ aqueous system. Figure 3(a) depicts the typical progressive absorption spectral changes in the Soret band region of *cis*-DMPyP in the WO₃ colloid aqueous solution under various pH conditions. The inset shows changes of the maximum molar absorbance coefficients at 372 (*H*-band) and 463 nm (*J*-band) depending upon the

pH values in the *cis*-DMPyP/WO₃ aqueous system. Upon increasing the pH value from 1 to 6, the *cis*-DMPyPs' *J*-dimer band at 463 nm was observed to disappear, and then a new *H*-dimer band at 372 nm appeared in the region higher than pH 3.5. Moreover, an isosbestic point was obtained at *ca.* 440 nm in the absorption spectra, implying stoichiometric conversion of *J*-dimers to *H*-dimers. In order to evaluate the reversibility of this color changing in the *cis*-DMPyP/WO₃ aqueous system, this pH titration was carried out over several cycles using the same solution, and the absorption spectrum was recorded after each step (pH 1.5 and 6.0). Figure 3(b) shows the variation of the maximum molar absorbance coefficients of *cis*-DMPyP in the acidic and neutral WO₃ aqueous solution, indicating the high degree of reversibility of pH-responsive color switching between *cis*-DMPyPs' *J*- and *H*-dimers formed on the WO₃ colloid surface. The *J*- to *H*-type aggregate transformation observed in this study originates from a change in the packing of the porphyrin cores on the WO₃ colloid surface. Hence, we surmise that this *cis*-DMPyPs' transformation involves the different location of the *N*-methyl-4-pyridyl substituent(s) and/or the different intermolecular interactions, since no pH-stimulus induces switching back and forth from *J*- to *H*-dimer in the *trans*-DMPyP/WO₃ aqueous system (not shown). The similar pH-responsive switching was also observed in the cationic/zwitterionic xanthen dye/WO₃ aqueous system as reported previously [27], indicating that protonation/dissociation of the xanthen derivatives adsorbed on the WO₃ surface induces reversible *H*- to *J*-aggregate transformation. Herein, we demonstrated that the drastic aggregation mode switching of *cis*-DMPyP dimers formed on the WO₃ colloid surface can be successfully achieved *via* controlling the external stimuli conditions, such as the pH change in the surrounding water medium. Recently, Eguchi *et al.* [49] investigated the orientation

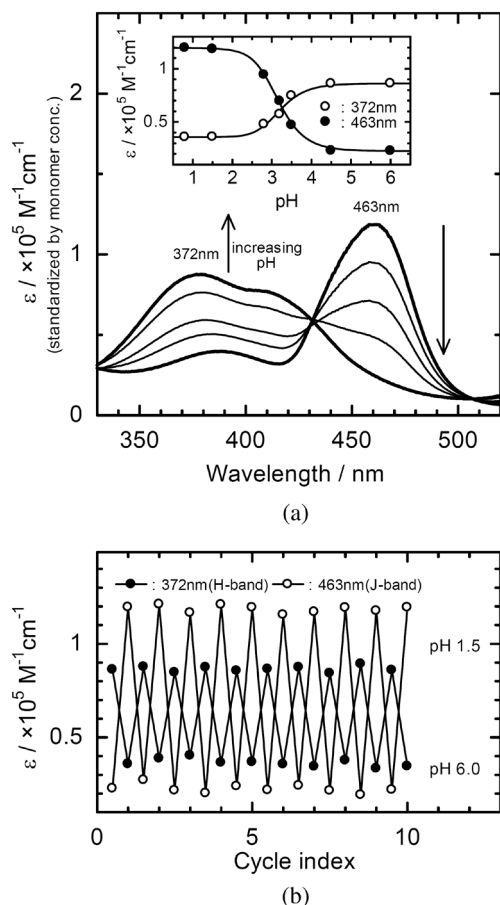


Fig. 3. (a) Change of absorption spectra in the *cis*-DMPyP/WO₃ aqueous system at 25 °C as a function of pH. Concentration conditions: [*cis*-DMPyP] = 1.0 × 10⁻⁶ M; [WO₃] = 1.0 × 10⁻³ M; [Na₂SO₄] = 3.3 × 10⁻² M. The arrows indicate the direction of the absorbance changes with increasing pH value. The insets show the molar absorptance coefficients at maximum wavelengths under various pH conditions. The lines in the insets are added as a visual guide. (b) Reversible switching between *H*- and *J*-dimerization in the *cis*-DMPyP/WO₃ aqueous system at 25 °C. Intensity changes in the molar absorptance coefficients at the *H*-band (filled circles) and *J*-band (open circles) maxima under 10 cycles of the acidic (pH 1.5) and neutral (pH 6.0) treatments

of *cis*-DMPyP molecules adsorbed on the synthetic clay (Sumecton SA) surface in various solvents, and likewise concluded that the tilting angle of *cis*-DMPyP with respect to surface could be reversibly controlled by changes in surrounding solvent environment. Although difference does exist in adsorbates and/or solvents, it is interesting that there is a similar trend for *cis*-DMPyP molecules adsorbed on the surface toward stimuli-induced conformational transformations.

Favorable geometry of DMPyP aggregates formed on the WO₃ surface

The UV-vis absorption spectroscopy has proven to be crucial and suitable for *in situ* quantitative information

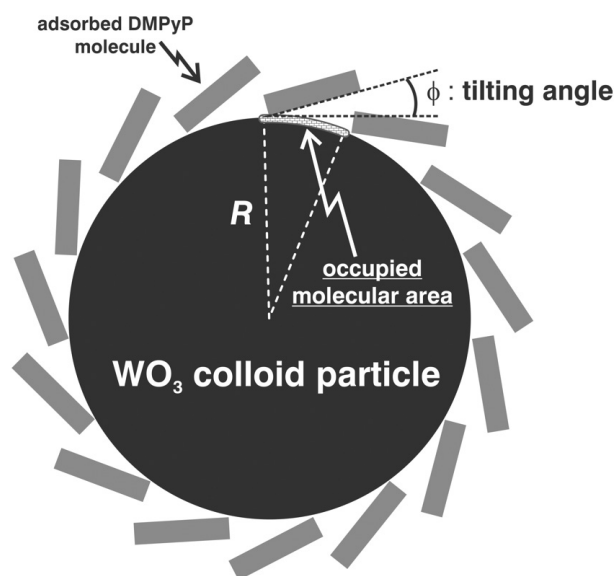
of the presence and orientation of the dye monolayer adsorbed on the metal oxide surface [27–29]. Therefore, the adsorption parameters of the DMPyP derivatives calculated for the Langmuir model evidence their energetically preferred adsorption geometries. Using the observed saturated concentration (*a*) values of DMPyP derivatives, the occupied area per molecule on the WO₃ colloid surface was calculated for every DMPyP/WO₃ aqueous system. For acidic and neutral *trans*-DMPyP/WO₃ aqueous systems, similar molecular area values were obtained (169 and 173 Å²/molecule, respectively). Because both experimental values are quite close to the projection area ones (estimated from the CPK model optimized at PM3 level with Gaussian 09 program [50]) of the *trans*-DMPyP derivatives lying flat-on (see Fig. 2(e)), a nearly flat-lying structure would be assumed for the monolayer adsorption/aggregation morphology of *trans*-DMPyP derivatives on the WO₃ colloid surface. The area per molecule in the acidic *cis*-DMPyP/WO₃ aqueous system was estimated to be 171 Å²/molecule, indicating that di-protonated *cis*-DMPyP molecules are also lying flat-on the WO₃ surface in the same manner as in the *trans*-DMPyP/WO₃ aqueous system. However, the area per molecule in the neutral *cis*-DMPyP/WO₃ aqueous system was 80 Å²/molecule, much smaller than that in the acidic same system, suggesting that the free-base *cis*-DMPyP molecules are standing perpendicular to the WO₃ colloid surface and adopt an edge-on arrangement for the situation of strong molecule–molecule (probably π–π) interaction. Consequently, this minimizes the interaction area with the underlying WO₃ substrate.

The primary mechanism through which molecular aggregate structures in the nature system are formed is generally self-assembly as a result of intrinsic intermolecular interactions [51]. Herein, depending on the DMPyP derivatives' geometric (*cis/trans*) isomerism and pH condition, we keenly observed various types of alignments that adopt either a “flat-on” or “edge-on” orientation of DMPyP derivatives with respect to the WO₃ colloid surface. Two different driving forces (not only the π–π intermolecular interaction between aromatic DMPyP moieties but also the electrostatic interaction between cationic DMPyP and negatively surface-charged WO₃ colloid particles) were used to assess the adsorption–aggregation behavior in the DMPyP/WO₃ aqueous system. As the WO₃ colloid particles used in this study are almost an ideal spherical shape with radius *R*, the adsorption onto curved surfaces should be considered. According to previous calculations [28], we can hypothesize and evaluate the probable arrangement for the DMPyP derivatives adsorbed on the WO₃ colloid surface, as shown in Scheme 3. Considering that the curvature radius *R* of WO₃ colloid particles nearly equals to 8.8 nm (from TEM image, Fig. S1), we predicted the molecular area (per DMPyP derivative) as follows (Equation 7):

occupied molecular area

$$\approx 2R^2 \tan^{-1}\left(\frac{l}{2R}\right) \tan^{-1}\left(\frac{l \sin \phi}{(l \sin \phi + R) \tan \phi}\right) \quad (7)$$

where l and ϕ are the length of the box approximating DMPyP derivative molecule calculated from CPK molecular model (see Fig. 2(e)) and the tilting angle of the porphyrin plane from the tangent line to a WO_3 particle surface, respectively. The ϕ values of *cis*- and *trans*-DMPyP derivatives, respectively, were estimated to be 20.3° and 20.9° in the acidic system (pH 1.5) and to be 87.2° and 22.6° in the neutral system (pH 6.0). For *trans*-DMPyP derivative, the tilting angles did not vary appreciably with a variation in ambient pH. In contrast, it is interesting to notice that the ϕ value in the neutral system was much larger than one in the acidic system for *cis*-DMPyP derivative. The present results, together with previously published studies [26–29, 52], clearly indicate that the adsorption arrangement of a porphyrin derivative adlayer on the metal-oxide surface is variable depending on the position of the electrically charged sites on each porphyrin derivative monomer. We already observed the paradigm for switchable red- and blue-shifted Soret band absorption in the *cis*-DMPyP/ WO_3 aqueous system depending upon pH. Given these facts and trends, it comes as no surprise that DMPyP derivative molecules adsorb onto the WO_3 colloid surface *via* the electrostatic interaction and then form ordered *H*-aggregates (face-to-face fashion) or *J*-aggregates (head-to-tail fashion) that reflect the intermolecular interactions.



Scheme 3. Schematic illustration of proposed model for adsorption of the DMPyP derivatives onto the WO_3 particle with radius R . Herein, the rectangles represent DMPyP derivatives

CONCLUSION

In summary, a detailed qualitative and quantitative study on the adsorption–aggregation of cationic porphyrin stereoisomers [5,10-diphenyl-15,20-di(*N*-methyl-4-pyridyl)porphyrin (*cis*-DMPyP) and 5,15-diphenyl-10,20-di(*N*-methyl-4-pyridyl)porphyrin (*trans*-DMPyP)] on the tungsten(VI) oxide (WO_3) colloid nanoparticle surface were investigated by spectroscopic method in combination with theoretical calculations (Langmuir adsorption isotherm and exciton coupling theory). Modified Langmuir isotherms in the DMPyP/ WO_3 aqueous system suggested that the DMPyP derivatives are adsorbed onto the negatively charged WO_3 colloid surface by the electrostatic interaction, and eventually form well-ordered dimers *via* diverse intermolecular interaction. Exciton-theoretical interpretation of spectral shifts has permitted us to discern that *cis*-DMPyP molecules in the acidic system (pH 1.5) formed the head-to-tail *J*-dimers on the WO_3 colloid surface (“flat-on” orientation with respect to the WO_3 colloid surface), whereas ones in the neutral system (pH 6.0) had a higher tendency to form the face-to-face *H*-dimers (“edge-on” orientation) unlike in the *trans*-DMPyP/ WO_3 aqueous system where *J*-dimers were always present regardless of pH conditions. More interestingly, we have experimentally demonstrated that the reversible switching between the *H*- and *J*-aggregation modes depending upon the pH value in the *cis*-DMPyP/ WO_3 aqueous systems. The findings obtained in this study may provide a good starting point for further development of more accurate models to control stimulus-responsive molecular alignment and orientation of various functional dyes on the metal oxide surface.

Acknowledgments

This study was partially supported by the “Regional Enterprise Support Foundation Project” sponsored by Yamaguchi bank and by the Scientific Research of the Grant-in-Aid for Young Scientists (B) (No. 24750069) and Scientific Research (C) (No. 16K05817) from Japan Society for the Promotion of Science (JSPS). ICP-AES and TEM measurements documented in this study were performed at the Center for Instrumental Analysis and the Innovation Center, respectively, Yamaguchi University.

The authors declare no competing financial interest.

Supporting information

Additional information, including Figs S1–S3, Table S1 (TEM image of the WO_3 colloid particles; concentration- and pH-dependence of UV-vis absorption spectra of DMPyP derivatives in water) and additional parameters of DMPyP derivatives’ aggregates in aqueous media are given in the supplementary material. This material is available free of charge *via* the Internet at <http://www.worldscinet.com/jpp/jpp.shtml>.

REFERENCES

- Paolesse R, Nardis S, Monti D, Stefanelli M and Natale CD. *Chem. Rev.* 2017; **117**: 2517–2583.
- Chakrabarty R, Mukherjee PS and Stang PJ. *Chem. Rev.* 2011; **111**: 6810–6918.
- Würthner F, Kaiser TE and Saha-Miller CR. *Angew. Chem. Int. Ed.* 2011; **50**: 3376–3410.
- Kobayashi T. (Ed.) *J-aggregates*, World Scientific Publishing: Singapore, 1996.
- Kobayashi T. (Ed.) *J-aggregates*, Vol. 2, World Scientific Publishing: Singapore, 2012.
- Bryant DA and Frigaard N-U. *Trends Microbiol.* 2006; **14**: 488–496.
- Sengupta S and Würthner F. *Acc. Chem. Res.* 2013; **46**: 2498–2512.
- Aziat F, Rein R, Peón J, Rivera E and Solladié N. *J. Porphyrins Phthalocyanines* 2008; **12**: 1232–1241.
- Arai Y and Segawa H. *Chem. Commun.* 2010; **46**: 4279–4281.
- Adachi K and Watarai H. *New J. Chem.* 2006; **30**: 343–348.
- Adachi K and Watarai H. *J. Mater. Chem.* 2005; **15**: 4701–4710.
- Adachi K, Chayama K and Watarai H. *Soft Matter* 2005; **1**: 292–302.
- Guo P, Zhao G, Chen P, Lei B, Jiang L, Zhang H, Hu W and Liu M. *ACS Nano* 2014; **8**: 3402–3411.
- Guo P, Chen P and Liu M. *Langmuir* 2012; **28**: 15482–15490.
- Mura S, Nicolas J and Couvreur P. *Nature Mater.* 2013; **12**: 991–1003.
- Hoffman AS. *Adv. Drug Deliv. Rev.* 2013; **65**: 10–16.
- Yan X, Wang F, Zheng B and Huang F. *Chem. Soc. Rev.* 2012; **41**: 6042–6065.
- Nakanishi T. (Eds.) *Supramolecular Soft Matter: Applications in Materials and Organic Electronics*, Wiley: New York, NY, USA, 2011 and references therein.
- Weingarten AS, Kazantsev RV, Palmer LC, Fairfield DJ, Koltonow AR and Stupp SI. *J. Am. Chem. Soc.* 2015; **137**: 15241–15246.
- Varghese R and Wagenknecht H-A. *Chem. Eur. J.* 2010; **16**: 9040–9046.
- Saparov B and Mitzi DB. *Chem. Rev.* 2016; **116**: 4558–4596.
- Butler KT, Walsh A, Cheetham AK and Kieslich G. *Chem. Sci.* 2016; **7**: 6316–6324.
- Arakaki A, Shimizu K, Oda M, Sakamoto T, Nishimura T and Kato T. *Org. Biomol. Chem.* 2015; **13**: 974–989.
- Gundlach L, Szarko J, Socaciu-Siebert LD, Neubauer A, Ernstorfer R and Willig F. *Phys. Rev. B* 2007; **75**: 125320–125328.
- Florio GD, Bründermann E, Yadavalli NS, Santer S, and Havenith M. *Soft Matter* 2014; **10**: 1544–1554.
- Adachi K, Mita T, Yamate T, Yamazaki S, Takechi H and Watarai H. *Langmuir* 2010; **26**: 117–125.
- Adachi K, Watanabe K and Yamazaki S. *Ind. Eng. Chem. Res.* 2014; **53**: 13046–13057.
- Kanetada N, Matsumura C, Yamazaki S and Adachi K. *ACS Appl. Mater. Interfaces* 2013; **5**: 12991–12999.
- Adachi K, Tanaka S, Yamazaki S, Takechi H, Tsukahara S and Watarai H. *New J. Chem.* 2012; **36**: 2167–2170.
- Zheng H, Ou JZ, Strano MS, Kaner RB, Mitchell A and Kalantar-Zadeh K. *Adv. Funct. Mater.* 2011; **21**: 2175–2196.
- Yamase T. *Chem. Rev.* 1998; **98**: 307–325.
- Yamamoto A and Adachi K. *Bunseki Kagaku* 2017; **9**: 639–646.
- Tanaka S, Adachi K and Yamazaki S. *Analyst* 2013; **138**: 2536–2539.
- Adachi K, Mita T, Tanaka S, Honda K, Yamazaki S, Nakayama M, Goto T and Watarai H. *RSC Adv.* 2012; **2**: 2128–2136.
- Lindsey JS, Schreiman IC, Hsu HC and Kearney PC. *J. Org. Chem.* 1987; **52**: 827–836.
- Rothmund P. *J. Am. Chem. Soc.* 1935; **57**: 2010–2011.
- Barrett EP, Joyner LG and Halenda PP. *J. Am. Chem. Soc.* 1951; **73**: 373–380.
- Brunauer S. *The Adsorption of Gases and Vapors*. Oxford University Press, Oxford, UK, 1944.
- Gouterman M, Rentzepis PM and Straub KD. (Eds.), *Porphyrins: Excited States and Dynamics*, ACS Symposium Series, American Chemical Society: Washington, DC, USA, 1987.
- Connors KA. *Binding Constants*, John Wiley & Sons: New York, USA, 1987.
- Okura I. *Photosensitization of Porphyrins and Phthalocyanines*, Gordon and Breach Science Publishers: Amsterdam, the Netherlands, 2000.
- Kadish K, Smith K and Guillard R. (Eds.) *The Porphyrin Handbook: Volume 1 Synthesis and Organic Chemistry*, Academic Press: San Diego, CA, USA, 1999.
- Kano K. *J. Porphyrins Phthalocyanines* 2004; **8**: 148–155.
- Kano K, Minamizono H, Kitae T and Negi S. *J. Phys. Chem. A* 1997; **101**: 6118–6124.
- Kasha M, Rawls HR and Bayoumi MA. *Pure Appl. Chem.* 1965; **11**: 371–392.
- Parks GA. *Chem. Rev.* 1965; **65**: 177–198.
- Kosmulski M. *Chemical Properties of Material Surfaces*. Marcel Dekker: New York, NY, USA, 2001.
- West W and Pearce S. *J. Phys. Chem.* 1965; **69**: 1894–1903.

49. Eguchi M, Shimada T, Tryk DA, Inoue H and Takagi S. *J. Phys. Chem. C* 2013; **117**: 9245–9251.
50. Wallingford, CT. *Gaussian 09 for Windows, Revision A.1*, Gaussian, Inc., 2009.
51. Lee YS. *Self-Assembly and Nanotechnology: A Force Balance Approach*, Wiley-Interscience: New York, NY, USA, 2008.
52. Fujii Y, Tsukahara Y and Wada Y. *Bull. Chem. Soc. Jpn.* 2006; **79**: 561–568.